Chapter 2

Design and Characterisation of *In Situ* Cells for X-ray Absorption Spectroscopic Investigations of Catalysts by Total-Electron Yield Detection

2.1. Introduction

All previous cell designs for catalysis studies by *in situ* X-ray absorption spectroscopy (XAS) relied either on transmission or fluorescence yield (FY) detection arrangements (for reviews see refs. [1,2], for more recent developments see refs. [3-19]). Both techniques impose a variety of experimental constraints. Most notable is their strict requirement of optically thin samples, which imposes sample preparation and measurement conditions (grinding, pellet pressing, etc.) which are unrepresentative of the active state of most catalysts in industrial practice. Moreover, even if a sample fulfills the nominal concentration requirements on a macroscopic scale, its microstructure may still be inadequate because of inhomogeneities. A particularly difficult problem arises when the particle sizes of the catalytically active components in the dispersion are too large. Particle diameters should be well below ~1 μm to ensure the absence of thickness- and self-absorption non-linearities [20] which distort the X-ray absorption fine structure (XAFS). The circumvention of these problems necessitates homogeneous dispersions and low concentrations of the element probed by the XAS experiment - requirements which are, particularly in the medium and soft X-ray ranges ($E < 10$ keV), only fulfilled by very low catalyst loadings and/or if the catalyst particle sizes are small. The recently developed arrangement for energy-dispersive XAFS [8,21-23] is additionally prone to XAFS distortions due to synchrotron beam movement over non-uniform samples [13,24,25].

Here, several *in situ* XAFS cells for catalysis studies will be described which operate by total electron yield (TEY) detection. Experimental results in subsequent chapters will show that TEY detection offers an elegant and inexpensive solution to several problems associated with the current state of *in situ* XAFS technology. An important advantage is the relative insensitivity (see also chapter 4) to XAFS amplitude distortions because the short escape depth of the signal electrons limits the probed sample thickness often (except at very low angles of incidence with respect to the sample surface and in samples with high fluorescence yields, see also chapter 4 below) to an optically thin layer. Highly concentrated as well as inhomogeneous

materials can be investigated reliably, simply by preparing samples thick enough to attenuate the entire incident X-ray beam. The present chapter will also demonstrate that *in situ* cell construction and operation are simple.

2.2. Previous Gas-Flow TEY Detector Designs: A Summary

In 1979, Shevchik and Fischer described the first gas-flow TEY detector [26] which simply consisted of a plexiglas box with 0.125 mm tungsten anode wire passing through its centre and openings for He flow and X-ray entry. The X-ray window was made out of commercial kitchen foil. The sample plate was glued to the inside base of the box, and the photocurrent passing through the sample measured by a grounded Keithley electrometer. The anode wire voltages were varied between 0 V and 1000 V, and the incident X-ray angle between 0° and approximately 15° with respect to the sample plate. This detector was utilised in studies of oxide films grown on copper and iron [26-29]. Several variations of this plexiglas type design have since been built and employed for TEY XAFS demonstration studies. Both anode wires [30-32] and anode foils, in particular aluminized mylar, have been used [33,34].

A major practical problem with plexiglas designs is the fact that they are prone to electromagnetic field interference due to the poorly shielding housing material. It is the author's experimental experience that the signal-to-noise quality achieved with unshielded detectors is inferior to data quality obtained with metallic housings. Unsurprisingly, several He-flow detectors based on metal casings have previously been described in the literature [35-38]. Their design concept followed the same principles as the plexiglas detectors described above.

More specialised cells with additional capabilities have been also been developed. The stainless steel cell of Elam *et al.* [37] combined vacuum with ambient pressure measurements. A diffusion pump system connected to the He flow system allowed evacuation to below 10^{-5} torr. Simultaneous fluorescence measurements were possible through an additional Kapton foil window. An all-metal cell by Tourillon *et al.* [36,39] was very similar in that it also allowed evacuation and fluorescence detection. Kemner *et al.* have constructed plexiglas cells which allow cooling of the sample by liquid nitrogen [40,41]. A very interesting recent development are TEY cells built by Watanabe *et al.* [42] which allow XAFS measurements at liquid surfaces. Obviously, such measurements also require an X-ray mirror for deflection of the incident X-rays onto the sample, as the gas-liquid interface is always horizontally aligned due to the gravitational field of the earth. Watanabe *et al.* have also built a versatile, miniature electron-yield cell made from metal for solid state studies mounted on a small two-axis goniometer to allow angle-dependent studies

[43]. A simple design for angle resolved single crystal studies was also described by Tylisczak *et al.* [35].

2.3. Environmental Cells for *In Situ* Studies of Catalysts by TEY XAS: Requirements

The essential parts of any gas-flow TEY cell are the collector and sample plates, which must be electrically insulated from the rest of the cell and connected to suitable, gas leak-tight feedthroughs. Furthermore, provisions must be made for X-ray photons to enter the cell through an appropriate window, and gas-flow must be maintained through in- and outlets. For an *in situ* catalysis cell it is desirable to fulfill additional requirements. Most important is the maintenance of *in situ* gas purity by sealing the cell volume from the external environment. A heating system must allow variation of the sample temperature. It must be stressed that no environmental cell can be ideally suited for all types of catalyst studies, because the range of catalytically active materials is vast, and *in situ* conditions vary according to the nature of the studied reaction. An instructive example of necessary considerations is given by the sample support plate. Its material must be chosen such that (i) it is not catalytically active itself, (ii) it does not react or alloy with a component of the catalyst investigated, (iii) it is stable under the reaction conditions employed (particular *caveats* being corrosion and/or thermal instability), and (iv) it does not contain the investigated element in the catalyst or any other element with an absorption edge in the energy range of interest. The list of further design constraints (e.g., choice of wall/window/tubing materials, window thickness, *in situ* pressure range, additional cooling of sensitive cell parts, etc.) is potentially long and depends critically on the choice of reaction system to be studied. The XAFS cells described in this chapter are designed in a modular way so that vital parts can be quickly replaced with the widest

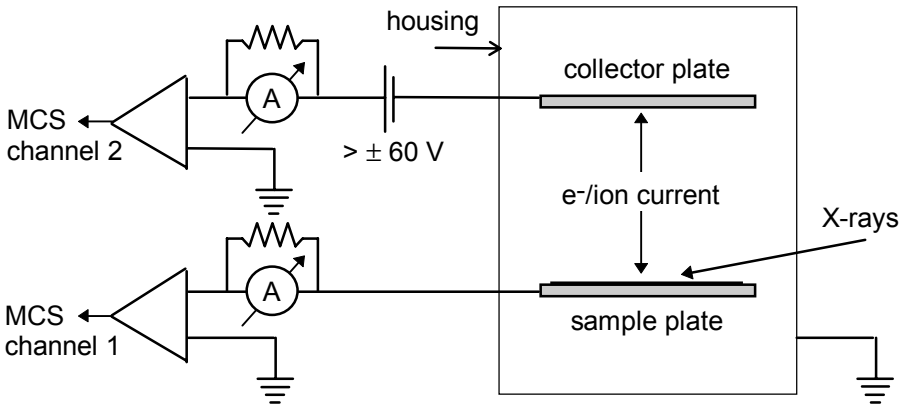

Figure 2.1. Schematic circuit underlying the gas-flow TEY experiment.

choice of materials. This design philosophy has proven to be successful for *in situ* X-ray diffraction studies with cells described in [6].

The circuit underlying the TEY experiment is simple (fig. 2.1). An electric field is maintained between the sample and collector plates of the detector by applying static voltages of approximately 100 V (note, however, that 60 V are often sufficient to ensure good signal-to-noise quality, see section 2.7 below). Low-noise biasing of the plates is achieved with a well-shielded, purpose-built stack of commercial 9 V and 1.5 V batteries. The polarity of the detector is not critical, but measuring the photocurrent from a grounded sample (while biasing the collector plate positively) has the advantage of minimizing distortions of the sample signal due to spurious photo- and secondary electron currents formed elsewhere in the cell, as the positively biased collector plate deflects all electrons from the sample and the cell housing. In experimental practice, the signals from both detector plates are fed directly into Keithley current pre-amplifiers. The voltage output produced by the current amplifiers is converted into a proportional frequency signal (with V/F electronics commonly used for transmission measurements) and recorded as a count rate in two single- or a multichannel-scaling device. After A/D conversion, the data are stored in the process computer. For further information on the requirements for the detection electronics the reader is referred to the work of Derbyshire *et al.* [44]. Simultaneous recording of both channels aids the identification of noise sources, a possibility which has previously not been explored. An instructive example of the information which can be extracted from the signal currents is given in fig. 2.2. Note that the experimental setup is essentially identical to a 2-channel fluorescence-yield detection arrangement, the only difference being that the electron-yield detector plates replace the fluorescence yield collectors. The TEY experiment is therefore readily carried out at any XAFS beamline which has facilities for fluorescence detection. In fact, if provisions for more than two fluorescence channels are available then the fluorescence signal from the sample can be recorded simultaneously.

All cells described in the subsequent sections were designed to be compatible with a purpose-built, transportable mounting table (overall dimensions approximately 40 cm × 20 cm). The table incorporates a single-axis goniometer onto which the cells are mounted. Remotely controlled stepper motors allow cell tilt variations of ±13° with respect to the horizontal position of the goniometer, and height variations within ±3 cm. Additional static displacements of the cell can be introduced with spacer plates and/or tilting the cell support on the goniometer. The remote control system enables *in situ* signal optimization and alignment by varying the position of the sample in the X-ray beam. *In situ* temperature control is achieved with a highly

stabilised Kenwood power supply (maximum output: 100 V/8 A) and a programmable Eurotherm temperature controller.

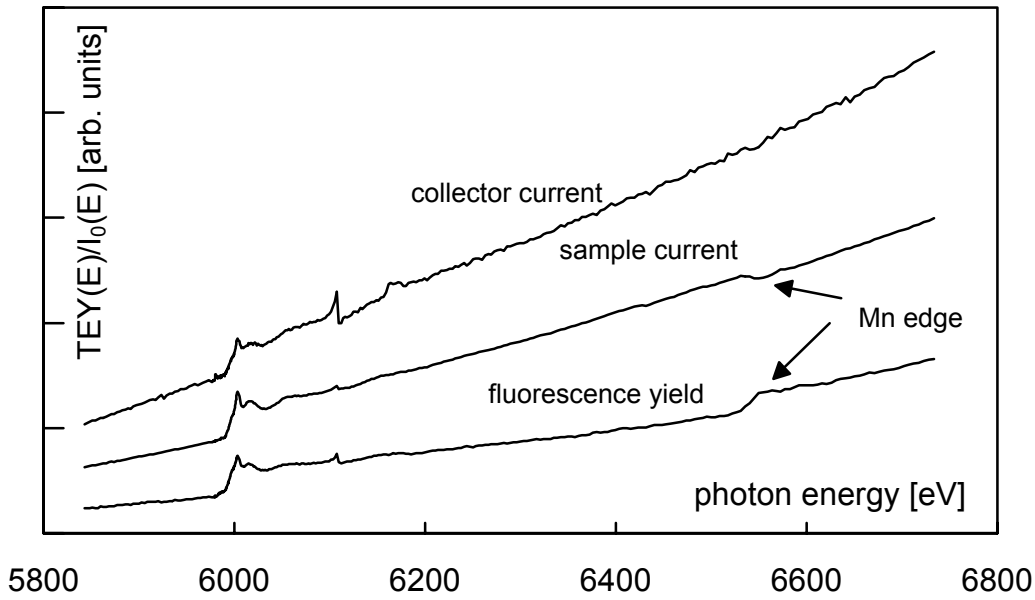

Figure 2.2. Cr K-edge single scan from a 10% Cr^{3+} promoter in an unsupported Cu model catalyst for the partial oxidation of alcohols. Fluorescence-yield and total electron-yield data from sample and collector plate were recorded simultaneously in the *in situ* cell described in section 2.6. (station 7.1. of the EPSRC Daresbury synchrotron, Si(111) monochromator, ring current: 170 mA at E = 2 GeV, scan time: 20 min, collector biased at +104 V). Note, how absorption by the Mn impurity in the Be vessel is visible in the fluorescence data (edge step) and in the electron-yield data from the sample (negative edge step, absorption). No Mn edge is observed in the collector current, probably because of fortuitious cancellation of the Mn TEY current collected from the Be vessel walls and the negative absorption edge step. Note also the reduced intensity of the Bragg glitch at 6100 eV in the sample current, and the low signal-to-noise quality in the collector current due to collection of spurious background signals.

2.4. Prototype Cell

This *in situ* electron-yield cell is based on a silica furnace tube around which is wound a NiChrome ribbon. Resistive heating of the NiChrome ribbon allows sample treatments at temperatures up to at least 800°C. A stainless steel metal foil (electrically insulated from the heating ribbon by a thin mica sheet) is placed between the silica wall and the NiChrome ribbon to afford some insulation against electromagnetic noise. The temperature is monitored by an Inconel sheathed thermocouple introduced into the furnace *via* a Swagelok coupling. At each end, the furnace tube is supported by a purpose designed water-cooled flange which also provide gas in- and outlets via 1/8" and 1/16" tubing with Swagelok connectors. Insulation from the external surroundings is made using Viton seals. Each water-cooled flange supports a second flange. At the front of the furnace tube, provisions

are made for supporting an X-ray window made of Kapton or Be tightly on a Viton ring. The end of the cell has a flange which enables electrical connection by vacuum-compatible ceramics feedthroughs. Studies at elevated pressures over 1 atm cannot be carried out in this cell. Purpose designed silica carriers support the sample and the collector plate, connection to the feedthroughs being made by bare wires (Au or Ni, 1 mm diameter) fused into the plates and *via* gold-plated crimp connectors. Plate materials are chosen according to experimental requirements: gold-plated silica, solid copper, solid nickel, and solid silver have all been used successfully in the studies reported in this thesis (note, however, that copper, nickel and silver can sometimes exhibit charging effects in oxidising environments at high temperatures as a result of corrosion).

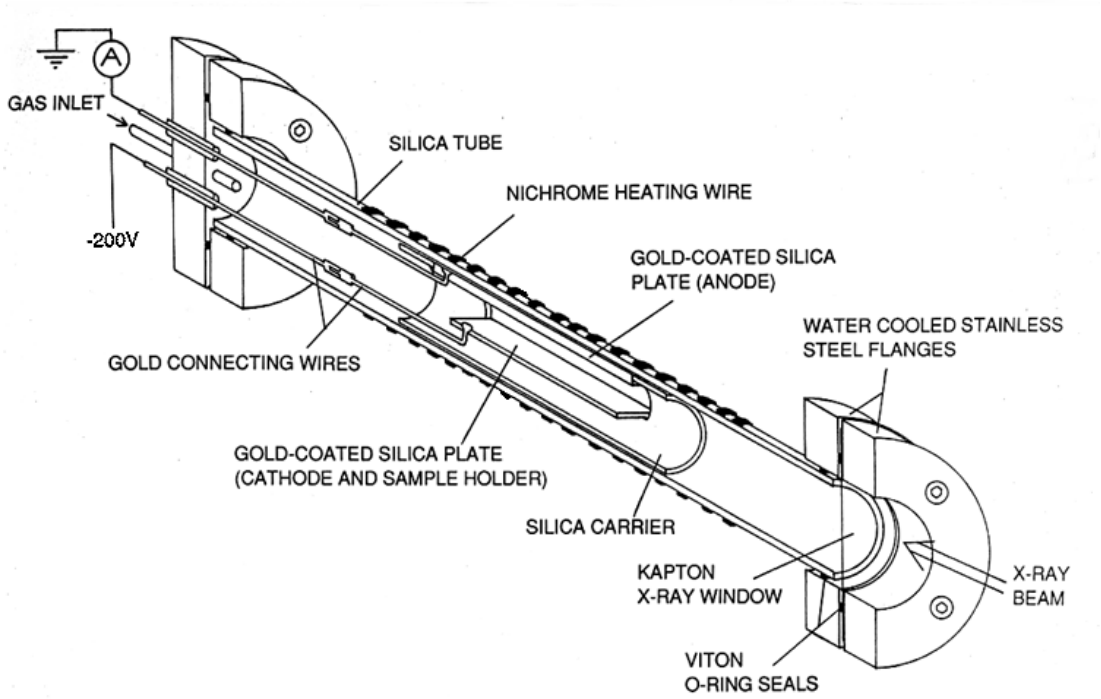

Figure 2.3. Schematic drawing of the prototype i*n situ* gas-flow electron-yield cell used for the study of materials at pressures of 1 atm and temperatures up to 800°C (from [6]).

This cell has been used in a variety of high temperature (T up to 800°C) studies at 1 atm pressure, including an earlier preliminary investigation of a methanol synthesis catalyst (60%Cu/30%ZnO/10%Al_2O_3) by Moggridge *et al.* [45]. The author has also carried out some measurements on annealed Ni wafers and Cu_5Ni_{95} particles in this cell. True *in situ* measurements at elevated temperature are possible, but results are noisy due to the electromagnetic field interference from the heating coil. High-temperature *in situ* data acquired in this cell will therefore not be presented in this

thesis. Much improved *in situ* noise levels were achieved with a new high-pressure, high-temperature cell described in section 2.6.

Apart from these limited *in situ* capabilities, the cell exhibits various other practical shortcomings. Firstly, the internal cartridge/plate/signal wire setup is mechanically very unstable and difficult to assemble due to strain in the connections to the feedthroughs. Secondly, the cooling-down period required after heating the cell to elevated temperatures is substantial (more than 30 min starting from 300°C-400°C) because of the large thermal mass of the cell and the low heat conductivity of the silica furnace. A faster response is desirable because it reduces the dead-time between heating/cooling cycles at the synchrotron. Finally, the cell geometry limits the angle of X-ray incidence to less than about 8° with respect to the sample. The requirement of low angles of X-ray incidence is limiting when flat samples are investigated because the TEY EXAFS amplitude acquired at low incidence angles is artificially reduced (see chapter 4).

2.5. Combined High Vacuum/Ambient Pressure Cell

This new cell (fig. 2.4.) has been designed by the author and is assembled around a standard 4-way cross tube made out of duraluminium, which has 40 mm (inner diameter) Klein flange (DN40KF) high vacuum seals based on Viton O-rings. The cell allows comparative electron yield measurements in vacuum ($p < 10^{-5}$ torr) and at 1 atm. Because no heating facilities were included in the original design, the plate supports could be conveniently machined out of acetal homopolymer (Delrin®, Polypenco Ltd.). Additional Delrin® rings inside the cell allow firm positioning of the removable plate carrier. Small, purpose-built Delrin® springs attach the sample plate ($40 \times 8 \times 1$ mm) firmly to the base of the carrier. X-rays enter the cell through a vacuum-tested, 0.1 mm thick Be window (sealed by a Viton ring), while a purpose-built end flange incorporates vacuum-compatible electrical feedthroughs and a 1/8" diameter gas inlet tube. A large diameter outlet allows connection of the cell to a turbomolecular pump. Also shown in fig. 3 is an optional Kapton window for simultaneous fluorescence yield detection of the XAFS. Recently, this window has been replaced by a vacuum compatible rotary drive which allows angle resolved studies. These measurements are carried out in the absence of all Delrin® supports and without a collector plate. Instead, the sample, mounted on a Ta foil support and located with small Ta springs spotwelded to the foil, is biased negatively to repel spurious electron signals formed elsewhere in the cell volume. The grounded cell housing acts as the collector. It is planned to introduce electrical feedthroughs which

will allow connection of an internal thermocouple and wires for resistive *in situ* heating of the Ta foil support.

This vacuum compatible cell demonstrates the simplicity of the experimental setup required for a gas-flow electron-yield experiment. The cell is ideal for non *in situ* measurements of standard samples, as it easy to assemble and align in the X-ray beam. In spite of now being used routinely for this purpose, this cell was initially conceived for comparative probing depth measurements in vacuum and in He (see ref. [46], and chapter 3). Furthermore, the influence of detector bias voltage and polarity, as well as detector gas composition on the XAFS results has been studied in this cell (see below).

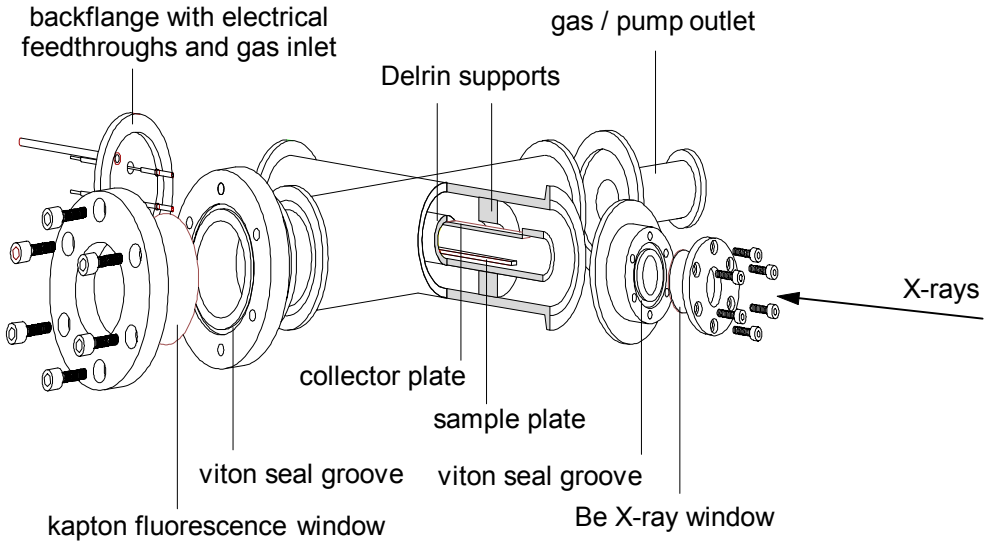

Figure 2.4. New combined high vacuum/gas-flow total electron-yield XAS cell for *in situ* studies of materials. The Kapton fluorescence window can be replaced by a 360° rotary sample manipulator for angle resolved studies of crystalline samples. For clarity, Viton seals and standard KF clamps have been omitted from the drawing.

2.6. High Temperature/High Pressure Cell

This cell was designed to address most of the shortcomings of the prototype TEY *in situ* cell described in section 2.4. In designing this cell, the following *desiderata* were considered essential features:

- simple assembly at the synchrotron, quick exchange and alignment of samples
- high pressure capability

- quick heating/cooling response
- good shielding against interference from electrical noise
- inertness of the wall materials, resistance against corrosive gases
- little catalytic activity in the cell materials
- simultaneous fluorescence yield detection

The resulting cell design is illustrated in fig. 2.5. The centrepiece of the cell is a miniature, disk-shaped sample-support block (16 mm diam., 5 mm height), which incorporates a printed platinum conductor circuit for resistive heating of the sample. The block itself is a sandwich made out of two laser-cut alumina disks (Hybrid Lasertech, Cambridge; alumina grade: Coors ADS 96R), which are joined with a sodium silicate cement (Autostic™, Carlton Brown and Partners, Sheffield). The bottom alumina plate (thickness 1 mm) supports the printed platinum circuit (resistance at room temperature: approximately 13 Ω) and contains laser-drilled holes (1 mm diam.) for heater wires, signal wires, and the gas inlet tube. A central hole (1.1 mm diam.) is provided for the introduction of a thermocouple (1 mm diam.) into the heating block. The upper plate (thickness 0.635 mm) simply contains matching holes for the gas inlet tube and the signal wires. The printed circuit was designed with a view to maximising the heat flux from the small available space, while minimising thermal strain in the alumina plate due to temperature gradients (previous rectangularly shaped heating circuits had cracked at temperatures of typically 300°C-400°C). The essentially centrosymmetric pattern was drawn with a CAD package, and a diapositive print was produced in the photographic workshop of the Department of Chemistry in Cambridge. The pattern was transferred from the print to a metallised wire screen (DEK1202 frame, MCI Ltd., Cambridge), which was used in printing the platinum circuit onto the alumina support plate (Cermet platinum conductor 5545, Agmet Ltd., Reading). Connection to the power supply is made by 1 mm diameter platinum wires, which were vacuum-brazed (Thermal Processing Group, Cambridge) to both ends of the printed circuit. The fully assembled heating block has been tested in air at temperatures up to 600°C. The power dissipated at this temperature is approximately 2 A@60 V = 120 W (note that the resistance of the Pt conductor increases with temperature). Power requirements in ambient gases which conduct heat well (H_2, He) can be considerably higher, limiting the available range of *in situ* temperatures to a maximum of 450°C. Heating and cooling rates are typically 80°C/min, reducing the dead-time between thermal cycles by an order of magnitude as compared to the prototype *in situ* XAS cell.

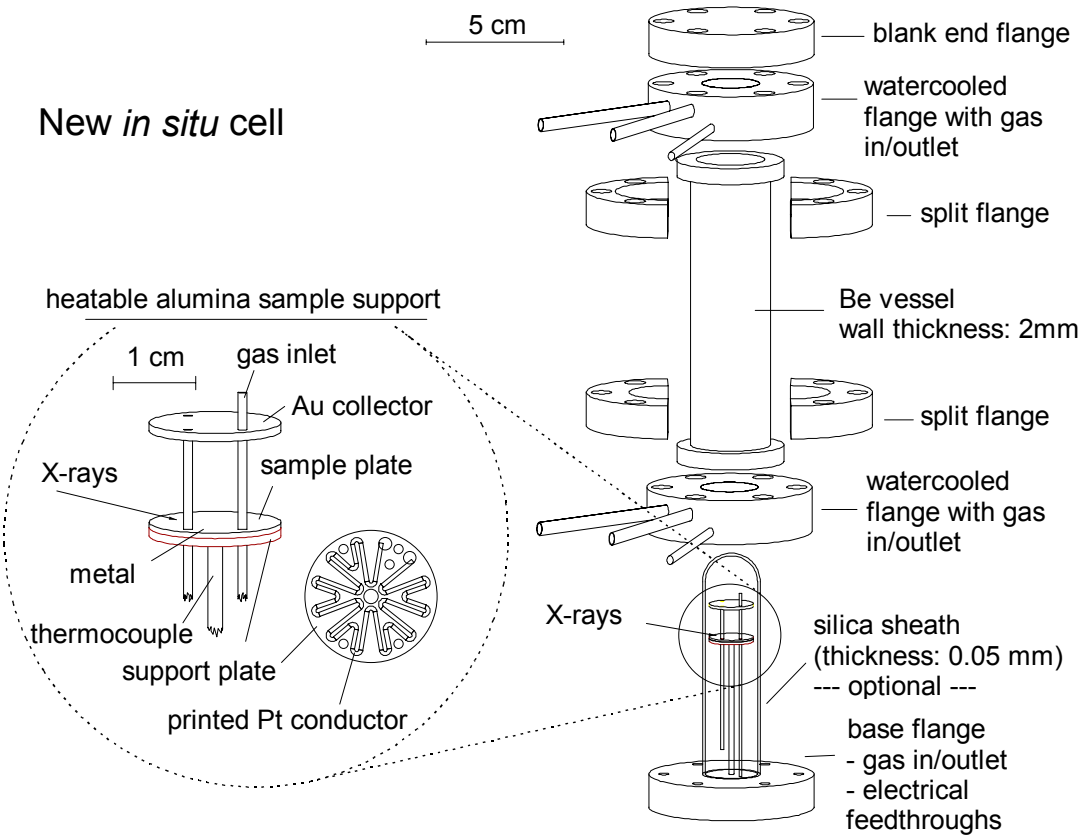

Figure 2.5. New gas-flow total electron-yield XAS cell for *in situ* studies of catalysts and other materials. For clarity, Viton seals have been omitted from the drawing.

The sample is supported by a metal foil, electrical connection being made by a platinum wire (0.1 mm diameter) spotwelded to the bottom of the foil. The foil material can be chosen according to *in situ* requirements. The collector plate is made out of inert material, usually a gold disk (16 mm diameter, 1 mm thick) which is electrically connected *via* platinum wire (0.1 mm diameter) crimped tightly into a small hole at the side of the disk. The collector plate is held in place by an arrangement of concentric alumina tubes around the gas inlet and signal wire tubes. Its distance to the sample can be varied by using alumina support tubes of different lengths, a possibility which is advantageous for XAFS measurements at high X-ray energies (above 10 keV) where the Auger electron penetration of light gases (H_2, He) can exceed distances over 1 cm (see section 2.7.4. below). A sample-collector spacing of 1.2 cm is fully sufficient for accurate gas-flow measurements at energies below 10 keV.

Platinum metal was chosen as the principal *in situ* wiring material since it is chemically inert against most corrosive atmospheres. It is, however, potentially active for many heterogeneously catalysed reactions, and is therefore shielded from the gas phase by alumina tubing (1 mm outer diameter). At the bottom of the cell, electrical

connections are made to Kapton coated copper wires (1 mm diameter) which reach the outside of the cell through 1/8" tubing and high-pressure compatible sealing glands (Deutsch Ltd.). The whole sample/collector assembly is supported by a thermocouple (1 mm diameter, inconel sheath, Philips-Thermocoax, Cambridge) fed through a sealing gland. The thermocouple is shielded from the gas phase by an alumina tube (outer diameter: 2 mm). Another alumina tube (1 mm diam.) serves as additional support and gas inlet, and is glued into the base flange of the cell (note that the base flange is water-cooled). Gas flow is maintained via 1/16" tubing vacuum-braised into the base flange, and sealed by Swagelok couplings.

At the heart of the outer cell body is a beryllium vessel (wall thickness: 2 mm) with a pressure rating of 80 atm. For studies at 1 atm, this beryllium vessel is usually replaced by a stainless vessel with a Kapton window. This has the advantage of avoiding experimental difficulties due to impurities in the beryllium (in particular Mn and Fe). For studies in environments which might potentially corrode the beryllium (moisture!), a silica thimble is used to shield the beryllium vessel against the active gas phase. The thimble is made from a quartz tube (wall thickness: 1 mm) which is closed on one end and drawn out such that a region approximately 40 μm thick results where the X-ray beam passes onto the sample. The experimentally determined transmission of the quartz window is approximately 50% at the iodine L_3-edge (4.5 keV). Because of the small window thickness, high pressure studies require the use of a differential gauge to apply equal pressures from both sides of the window (external gas: helium).

The cylindrical geometry of the cell allows positioning of an additional fluorescence-yield detector close to the catalyst. This is useful for measurements of diluted components in the catalyst, for which the signal-to-background ratio of the electron-yield signal is insufficient. Good shielding against electrical noise from the environment is achieved by the all-metal design of the cell. The metallic sample support foil also shields efficiently against electrical interference from the heater circuit underneath (the residual noise allows meaningful *in situ* measurements up to at least 600°C). Alignment of the sample is routinely achieved by use of a laser tracing the synchrotron beam path. The sample block remains exposed during the alignment procedure, allowing quick and simple positioning of the sample in the beam. After full assembly of the cell the sample position can be fine-tuned *in situ* with the remote-controlled stepper motor system briefly described in section 2.3.

The functionality of this cell will be demonstrated in chapters 5-6 of this thesis which will describe the results of *in situ* studies of Cu/Ni alloy model catalyst and a high-pressure study of a $Cu/ZnO/Al_2O_3$ methanol synthesis catalyst. Phase transitions

during the calcination of hydrated chromium hydroxide and of catalyst precursors containing a chromium hydroxide promoter have also been studied in this cell (results not presented in this thesis). The cell is amenable to QEXAFS experiments with a quick-scanning monochromator. An example of simultaneous fluorescence-yield/electron-yield detection has already been presented in fig. 2.2. This cell establishes a major step forward in electron-yield XAFS *in situ* technology. In particular the simplicity of the setup and the fast thermal response have substantially increased the speed of experimental sample throughput.

2.7. Influence of Detector Bias and Polarity

2.7.1. Introduction

Relatively little attention has previously been devoted to the influence of the detector characteristics on the TEY signal emitted from the sample. It is important to realise that the gas-flow TEY signal is fundamentally modified by charge-multiplication processes occurring in the gas phase. We will see in chapter 3 that comparing the vacuum and gas-flow signals from the same sample provides fundamental information on the TEY signal, particularly the average kinetic energy carried by the electrons. Knowledge of the TEY signal response to the applied bias voltage will be a prerequisite for the interpretation of data for the TEY signal attenuation in NiO overlayers. This section presents the results of an investigation into the TEY signal variation as a function of the detector bias voltage, its polarity and the ambient gas-pressure.

2.7.2. Physical Principles of Gas-Flow Ionisation Chambers

The gas-flow TEY cells described in this thesis are essentially ion chambers with an internal photoemitting sample. Ionisation detection of energetic electrons involves the removal of one or more electrons from gas atoms/molecules in the chamber volume *via* impact ionisation events. Each ionising collision between an energetic electron and a gas particle produces a positively charged ion and an additional electron. Both particles, due to their opposite charges, attract one another. In an electric field of sufficient strength, recombination is prevented by instant acceleration in opposite directions along the electric field lines. The energy required to create such an electron/ion pair has been measured for a wide variety of gases. An important result of these studies is the observation that the pair formation energy is, for most gases, almost independent of the incident electron energy [47]. Furthermore, the

energy loss necessary for pair formation varies little between gases; typical values are 30 ± 15 eV [48,49].

Depending on the magnitude of the applied voltage, ionisation chambers can be operated in several regimes. In the highest voltage region (the so-called Geiger-Müller region, applied potential more than several keV), very high electric field strengths result in intense field-acceleration of the emitted electrons [48,49]. saturated discharge pulses are formed, the intensity of which being independent of the initial number of charges formed by the detected signal electrons. This region is of little relevance to the present study because the gas-flow TEY detectors were always operated far below the Geiger-Müller voltage threshold.

The lower-voltage region includes the proportional- and the current mode regimes. The proportional region is similar to the Geiger-Müller region, in that field acceleration allows the formation of additional charges *via* impact ionisation of the collision partners. However, the intensity of each charge pulse is proportional to the number of charges which would be formed by each electron in the absence of an electric field. Increasing the field strength in the detector increases the measured pulse height signal. Results of such measurements will be described in section 2.8, but all other data presented in this work were collected at even lower voltages, in the so-called current regime.

The current regime applies at voltages between 60 V and 200 V - below the threshold at which any additional charges due to field-induced pair formation can be formed. *Here, the signal strength is independent of the detector voltage*, and any gas amplification of the TEY signal relative to vacuum detection must have its origin in excess kinetic energy carried by electrons emitted from the sample. The signal amplification factor obtained by filling the space over the photoemitting sample is therefore a measure of the kinetic energy content of the TEY. This linear relation between the electron energy and the gas-amplification factor will be exploited in the analysis of depth attenuation experiments described in chapter 3.

Finally, note that a non-linear, noisy response of the detector occurs at very low voltages (less than 40 V) where electron-ion recombination processes are possible [48,49].

2.7.3. Experimental

The experiments were carried out with the prototype cell (gas-flow measurements) and the high-vacuum cell (all other measurements) described above. Pure He gas (purity: 99.99%) was chosen as the detector gas because its low absorption coefficient makes it the preferred detector medium for gas-flow TEY investigations.

An oxidised (NiO thickness about 400 Å) Ni-wafer was the test sample. Measurements were carried out on stations 8.1 (vacuum detection) and 9.2 (gas-flow detection) of the Daresbury synchrotron with beam currents between 160 mA and 200 mA (E = 2 GeV). Harmonic rejection was performed by detuning the double Si(220) monochromators to 50% of maximum reflectivity. The incident angle of the X-ray beam with respect to the sample was 5°±2°. Only near-edge spectra were recorded. In the vacuum experiments, a Penning gauge for monitoring the pressure was placed on the flange opposite to the pump outlet of the vacuum cell. Measurements were carried out first by biasing the sample with positive and negative potentials, and then repeating the measurements with the bias on the collector plate. The edge step height was taken as a measure of the signal intensity. It was determined graphically, placing linear backgrounds through the pre-edge and post-edge regions and calculating the edge-step height. The estimated error in the edge step currents determined by this method is within ± 10% for gas-flow detection, but significantly higher for vacuum, especially at low voltages, due to the overall much lower signal intensity (signal-to-noise levels at low voltages are poor and the spectra are severely distorted).

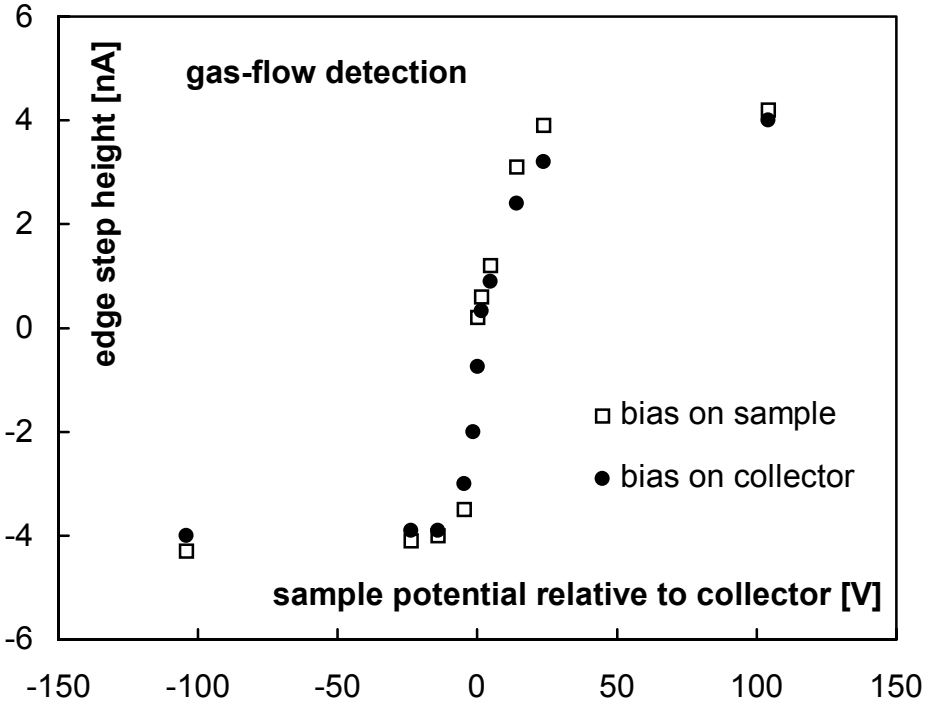

Figure 2.6. Ni K-edge step height in a gas-flow TEY detector as a function of bias voltage and polarity. The results represent the measurement of the current from the sample. Note that the open squares correspond to measurements with a biased sample, while the filled circles represent measurements with a biased collector plate. The ordinate is given in terms of the sample potential with respect to the collector. A negative (positive) collector voltage therefore corresponds to a positive (negative) bias of the sample.

2.7.4. Results and Discussion

The bias characteristics of the gas-flow detection mode are given fig. 2.6. The results indicate clearly that the current regime, where the detected TEY signal is independent of the bias voltage, is reached at detector field strengths corresponding to about ± 25 V, independent of polarity and position of the biasing battery in the circuit. The data in fig. 2.6. show that the current mode regime extends, independent of bias and polarity, over a region of at least 75 V, indicating that field inhomogeneities in the parallel plate detector are negligible.

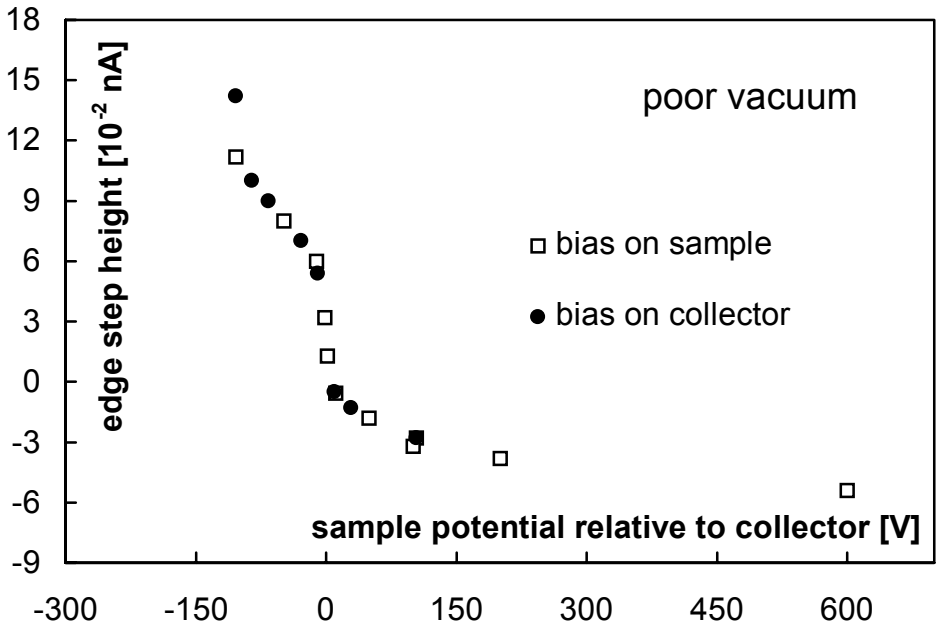

Figure 2.7. Ni K-edge step height in a poorly evacuated TEY detector as a function of bias voltage and polarity. The results represent the measurement of the current from the sample. Note that the open squares correspond to measurements with a biased sample, while the filled circles represent measurements with a biased collector plate. The ordinate is given in terms of the sample potential with respect to the collector. A negative (positive) collector voltage therefore corresponds to a positive (negative) bias of the sample.

The situation changes markedly when the detector is operated at slightly reduced pressures (fig. 2.7). An intermediate pressure range was achieved by leaking some ambient air into the system so that an internal pressure of about 10^{-2} torr resulted. The overall TEY signal strength dropped by about one order of magnitude. Furthermore, the voltage dependence of the TEY signal was asymmetric with respect to 0 V. When the sample is at negative potential with respect to the collector, good signals can be achieved with voltages around 25 V. A current-mode regime is not discernible anymore because the mean free path between collisions is now large enough to allow additional impact ionization events in the residual gas of the detector. As a result, the detector operates in a quasi-proportional mode at bias

voltages below 50 V. Reversing the detector polarity does not result in the loss of the TEY signal (as would be expected in high-vacuum, at least when secondary electron contributions emitted from the detector housing are absent), but in a residual signal which increases with applied voltage. This is due to the collection and gas amplification of (secondary) electrons emitted in collisions between Auger electrons and internal cell walls.

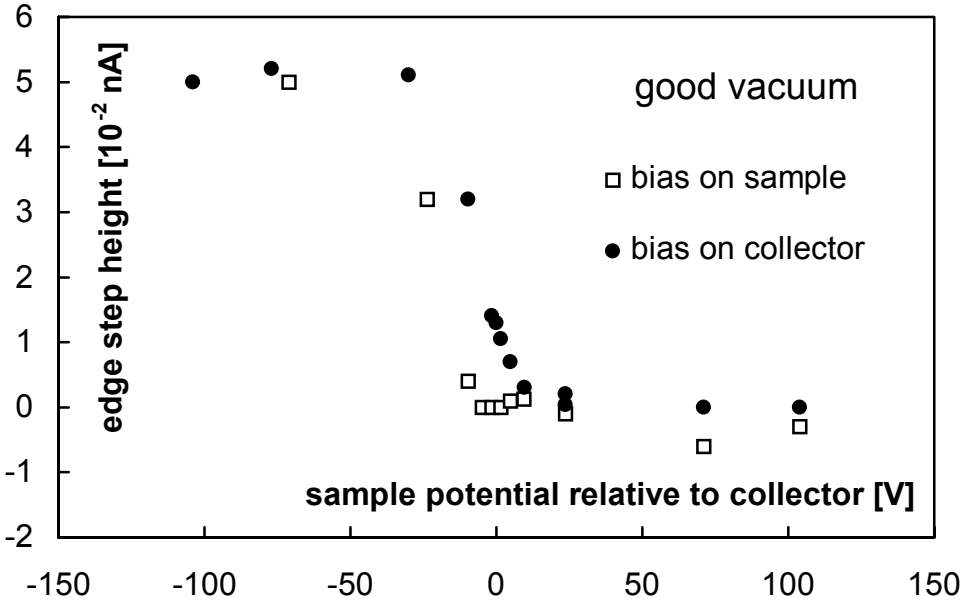

Figure 2.8. Ni K-edge step height in a TEY detector operating in high-vacuum as a function of bias voltage and polarity. The results represent the measurement of the current from the sample. Note that the open squares correspond to measurements with a biased sample, while the filled circles represent measurements with a biased collector plate. The ordinate is given in terms of the sample potential with respect to the collector. A negative (positive) collector voltage therefore corresponds to a positive (negative) bias of the sample.

Under good high-vacuum conditions ($p < 10^{-5}$ torr, fig. 2.8), the TEY current is very low when the sample is positively biased with respect to the collector plate. Very few electrons have sufficient kinetic energy to leave the electric field around the sample plate. Interestingly, however, the current is not *entirely* suppressed - an observation which has already been made already by Erbil *et al.* [50]. These authors tried to establish that low-energy ($E < 20$ eV) secondary electrons dominate the TEY current measured under vacuum conditions. A substantial *reversed* current upon placing a strong positive bias on the sample clearly contradicts any *a priori* assumption that secondary electrons prevail overwhelmingly in the total current, because the kinetic energy of secondary electrons is insufficient to allow them to escape from the attractive electric field. The only TEY contribution which could be responsible for the reversed current are the energetic Auger electrons because only they carry enough

energy (Ni KLL electrons: 6.5 keV) to escape from the attractive field. The reversed signal current through the sample must therefore be due to the collection of secondary electrons emitted from the detector housing materials during bombardment with Auger electrons. Erbil *et al.* resorted to explaining the reversed current in terms of the ionisation of residual gas particles in their vacuum chamber. However, this explanation is physically non-sensical, as the collision mean free path of Auger electrons in the pressure range used for their measurements (approximately 10^{-5} torr) is longer than their (and the present) vacuum chamber dimensions.

Application of a *negative* bias to the sample yielded, except at very low voltages (< 20 V), very satisfactory TEY signals. Certainly, this result is expected, as this is the configuration which has been used in TEY studies for more than two decades. The negative potential ensures that no photoemitted electron returns into the sample specimen. However, efficient collection of all emitted electrons is also achieved by accelerating all emitted charges towards the collector plate. The maximum TEY signal current (0.05 nA) for this polarity is achieved by electric field strengths corresponding to a collector bias of approximately +25 V.

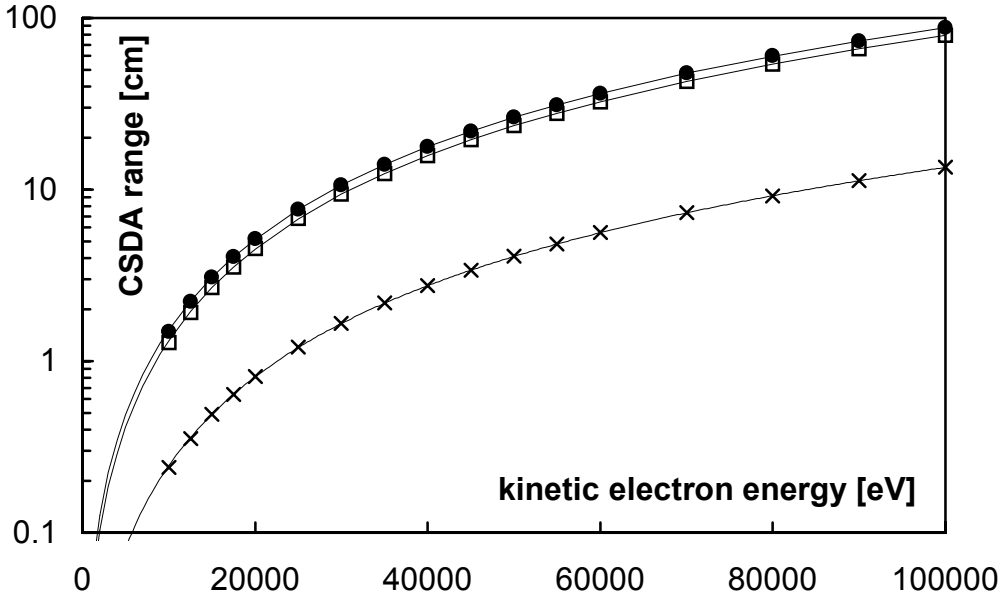

Figure 2.9. CSDA (continuous slowing-down approximation) range of electrons in 1 atm of He (filled circles), H_2 (open squares) and air (crosses) as a function of kinetic energy. The symbols represent the values recommended in [52]. The lines are fourth order polynomial fits to the data (extrapolated at energies below 10 keV assuming that the intercept is zero).

Having identified the important rôle of collisions between Auger electrons and wall materials, the question arises whether such contributions are non-negligible in gas-flow experiments. In other words, it should be useful to know under which conditions energetic Auger electrons penetrate the gas phase and excite additional

secondary charges in the internal detector materials. An answer can be found by inspection of the literature on electron impact ionisation cross sections [51] and electron mass attenuation data [52]. The influence of strongly penetrating electrons is expected to be most pronounced for He and H_2, as these gases have the lowest cross sections for electron impact ionisation [51]. An upper limit for the electron penetration in these gases is given by the *total electron ranges* [52], which give the total pathlength that an electron of given kinetic energy travels before it has thermalised all its excess energy. The graph in fig. 2.9 contains values for He, H_2 and air (all derived using the continuous slowing down approximation, CSDA, which is introduced in more detail in section 3.7) as well as 4th order polynomial fits to these data. It is clearly seen that an electron with an initial kinetic energy of 10 keV never travels a total distance exceeding 1.5 cm before coming to rest. The true penetration range is lower than this. Calculations in chapter 3 will show that the actual penetration range is rarely larger than 60% of the total range, as the electron path is not straight but randomised through elastic and inelastic collisions in the gas phase.

The important conclusion to derive from figure 2.9. is that the electron penetration in H_2 and He can become of the same order of magnitude as practical TEY detector dimensions. If the effect of secondary electron production due to collisions with the detector walls and collector plate are unwanted, then care must be taken to allow enough space for the energetic Auger electron contributions to dissipate their kinetic energy. As a rule of thumb, a distance of 1 cm should be fully sufficient for electron energies in the range below 10 keV (this range covers the KLL Auger electron energies in the periodic system up to approximately Br). The measurement of accurate gas-flow amplification data for the K-edges of heavier elements requires larger sample-collector spacings. Of course, the distance requirement is much less stringent when heavier detector gases are used: figure 2.9 shows that the electron penetration through air is about one order of magnitude shorter than in H_2 and He.

2.8. Pulse Count Detection: Useful for *In Situ* Studies?

2.8.1. Introduction

In theory, some energy discrimination between the photoemitted electrons can be achieved by operating the gas-flow TEY detector as a proportional counter. The proportional region of an ionisation detector is reached when the strength of the electrical field in the counter exceeds the limit where the acceleration of electrons and ions between collisions with neutral gas particles is strong enough to allow additional impact ionisation events [48,49]. The height of the field-amplified charge

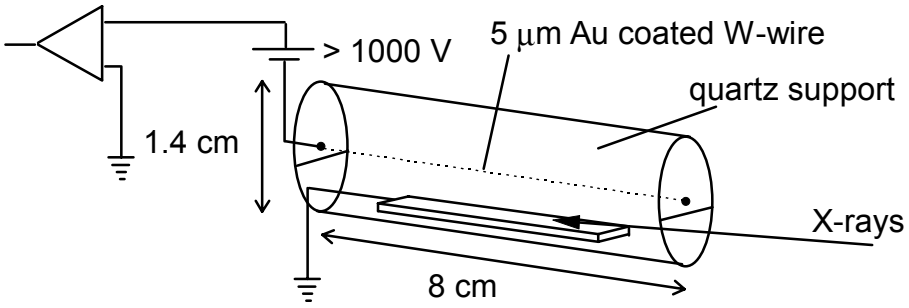

Figure 2.10. Schematics of the quartz support 'cartridge' used for pulse counting experiments in the cell described in section 2.4.

pulses is proportional to the initial energy of the electron entering the detector. The pulse height distribution function resembles an X-ray photoelectron spectrum convoluted with the resolution function of the proportional detector and some energy discrimination can be achieved *via* pulse height discrimination [32,53]. The average energy of the emitted electrons is related to the depth of their origination point in the sample: the deeper the region from which the electron escapes, the more inelastic collisions it will have undergone before reaching the surface. High-energy contributions to the emission spectrum therefore carry more surface sensitive information than low-energy contributions (note that extremely surface-sensitive elastic Auger electron contributions below 1 keV cannot be reliably detected by this technique). Accordingly, the surface sensitivity of pulse count detection could be enhanced by recording only the elastic and quasi-elastic contributions to the spectrum, and choice of different energy windows could in principle provide information on compositional and structural changes in the sample as a function of sampled depth. Using this approach, Bedzyk and Materlik have demonstrated how the composition of SmS changes from a highly defective Sm^{3+}-containing region at the surface to the stoichiometric bulk composition characterised by Sm^{2+} [53].

Because of these additional features, the pulse-counting technique could be a particularly valuable tool for the study of near-surface morphology changes in samples under reaction conditions. To explore the possibilities of proportional counting further, a trial experiment was made to test the technique's performance under mild *in situ* conditions.

2.8.2. Experimental

Experiments were carried out in the prototype cell described in section 2.4. The sample was mounted in a purpose-designed quartz support (fig. 2.10.) which carried a standard Au-coated W-wire (5 μm thickness, Goodfellow Ltd.) connected to a high-voltage supply. A high-voltage compatible preamplifier (circuit design by G. Salvini,

EPSRC Daresbury Laboratory) was used to process the raw detector output. The preamplified signal was directed into an EG&G 570 pulse-shaping amplifier (shaping time: 3 μs). The negative NIM output of the shaping amplifier was fed into an array of single-channel analysers tuned to the desired pulse height ranges. The signal from each channel was recorded as a separate spectrum. Note that the electronics hardware is practically identical to that used with multi-array solid-state fluorescence detectors (see, e.g., ref. [44]). The only addition to the standard fluorescence-yield setup is the high-voltage compatible preamplifier.

Data were collected in November 1993 on the focused beamline 8.1 of the EPSRC Daresbury synchrotron facility operating *in single bunch mode* at 2 GeV energy and with electron currents between 15 mA and 35 mA. The incident beam intensity was monitored by an ion chamber containing a mixture of He and Ar (80% transmission at the Ni K-edge). Using Co and Al foils in front of the ion chamber, the beam was attenuated to approximately 1/10 of its full single-bunch intensity to circumvent saturation of the proportional counter. Count rates of typically 2000 s^{-1} were thus obtained. A double-crystal Si(111) monochromator was tuned to 50% of maximum reflectivity to reject beam harmonics. Its piezoelectric actuator system which, under multi-bunch beam conditions, is normally used to minimise low-frequency fluctuations of the incident beam intensity [54] was switched off because the feedback system proved unstable due to beam movement and/or low beam intensity in the reference ion chamber. Several gases were investigated for their pulse-counting compatibility (10% CO_2 in He, pure He, 10% CO in He, all obtained from ECM, 99.99% pure). A diamond-polished Ni wafer covered by 220 Å of NiO (experimental details of the preparation and oxide thickness analysis can be found in section 3.3. and Appendix A) was used as a test sample.

2.8.3. Results and Discussion

Figures 2.11. and 2.12. compare a representative pulse dataset (recorded in 10% CO_2/He) to He gas-flow data (recorded in multi-bunch mode with a beam current of 189 mA under otherwise identical conditions prior to the single bunch experiment). The collection time for both spectra was identical (40 min). The signal-to-noise quality of the pulse spectrum is quite satisfactory, especially if one takes into account that the beam intensity during the experiment was about two orders of magnitude lower than in the comparative TEY measurement in current mode. Both normalised near-edge spectra (fig. 2.11) and the extracted EXAFS functions (fig. 2.12) reveal that the structural information obtained in the spectra is, within the signal-to-noise limits, identical. This result is as expected since the presented pulse spectrum is comprised of almost all spectral contributions to the TEY. Its information content

should therefore be identical to the information carried by the photocurrent. Note however, that pulse contributions at very low energies (below approximately 1000 eV) had to be filtered out from the spectrum, as it was observed that the XAFS information in this region was strongly distorted/attenuated. This is illustrated in figure 2.13, which shows that an edge-step can clearly be seen in the low-energy data, but no fine-structure. The origin of the absent XAFS information is presently not entirely understood. It is probably an experimental artifact, possibly reflecting some unidentified saturation effect in the detection electronics for low pulse heights. In view of the fact that Bedzyk and Materlik have previously [53] collected meaningful data in this low-energy region, this explanation seems quite likely.

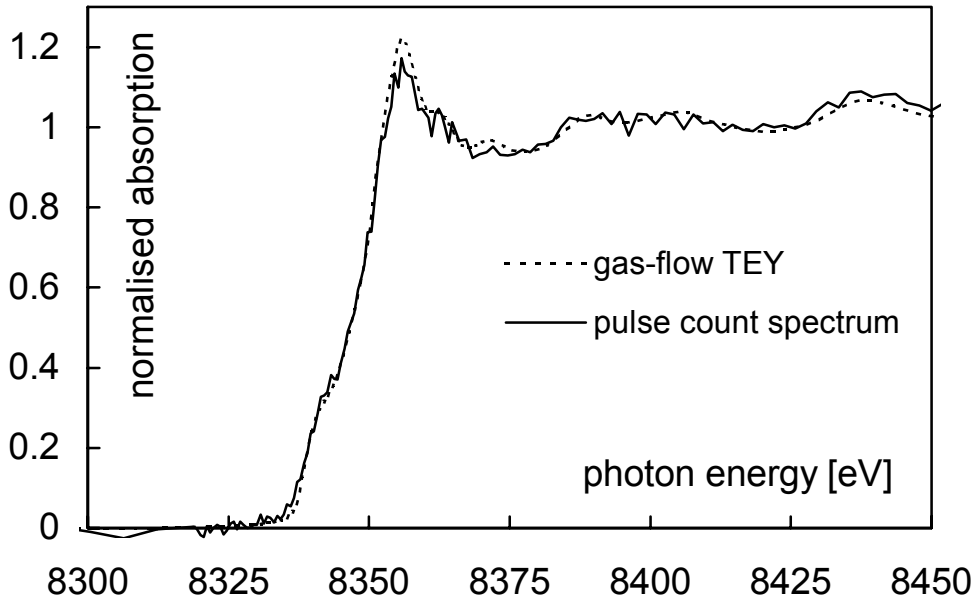

Figure 2.11. Normalised pulse-count- and gas-flow TEY spectra of a Ni wafer covered by 220 Å of NiO.

Unfortunately, depth resolution could not be obtained with the described experimental setup. In general, severe experimental difficulties in obtaining pulse-counting spectra were encountered as a result of spark formation, wire erosion, and slow gas-composition changes during the experiment. Wire erosion is a particularly fundamental problem, as whiskers on the wire induce an inhomogeneous electric field in the detector. A direct result of this is the occurrence of sparks in the detector volume, which aggravate the problem further due to increased erosion of the wire. Pulse height drifts resulted from gas composition changes and made long data collection times impossible without regular retuning of the detector, typically on a time scale of 30 min or so. When erosion processes had set in, the period of stability became even shorter. Spark formation also created difficult design challenges for the preamplifier electronics; during the present experiments, the preamplifier was

repeatedly damaged by spontaneous gas discharge. Sparking problems can, in principle, be alleviated by using appropriate gas-mixtures, such as the self-quenching 10% CH_4 / 90% He mixtures commonly used in proportional detectors for X-ray diffraction [49,55,56]. However, choice of self-quenching gases limits the applicability of the pulse-counting technique for *in situ* studies of catalysts severely.

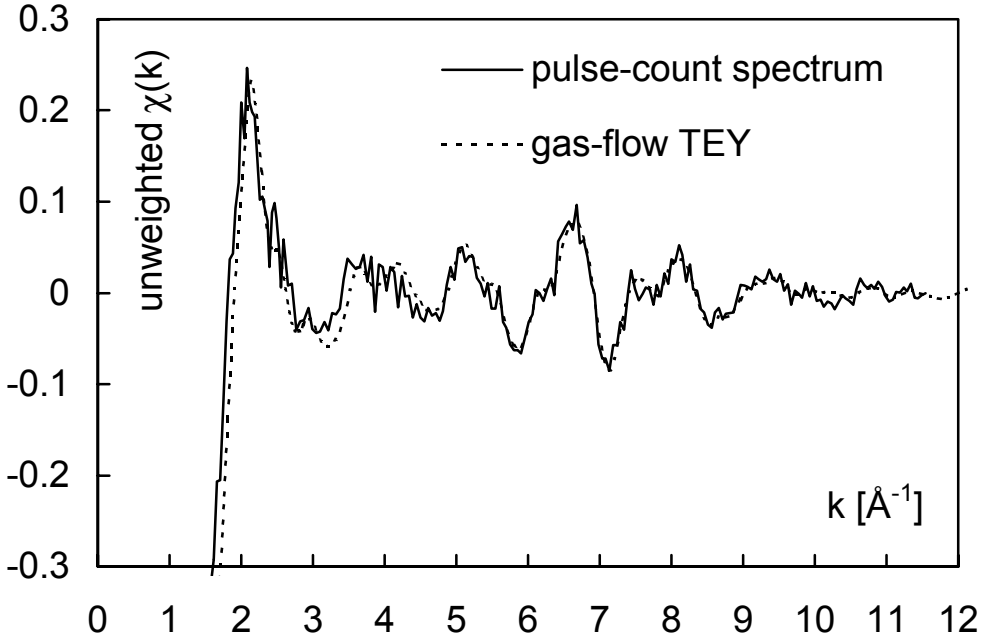

Figure 2.12. XAFS functions derived from the spectra contained in fig. 2.11. Note that pulse-count and He gas-flow EXAFS are identical within the signal-to-noise limits.

In summary, it has been shown that energy-resolved measurements *via* proportional detection are in principle feasible using the multi-channel fluorescence-yield electronics which are present at many XAFS beamlines. Single-bunch beam is satisfactory because the maximum count rate permissible in the proportional detector is very low compared to typical synchrotron beam intensities: in fact, even the single-bunch beam had to be attenuated by an order of magnitude. This is an important advantage of the technique since the demand for single-bunch XAS beamtime is usually limited, hence a generous allocation is often available at synchrotron facilities. The reported pulse-counting experiment has only been a first step towards a more thorough development of a potentially powerful technique. However, given the immense complications which were encountered due to spark formation, gas composition changes and anode erosion, it can already be concluded that the approach is unlikely to be useful as an *in situ* XAFS acquisition technique. Future work should refine and extend the limited experimental know-how about the pulse-counting technique for surface-sensitive *ex situ* studies of materials.

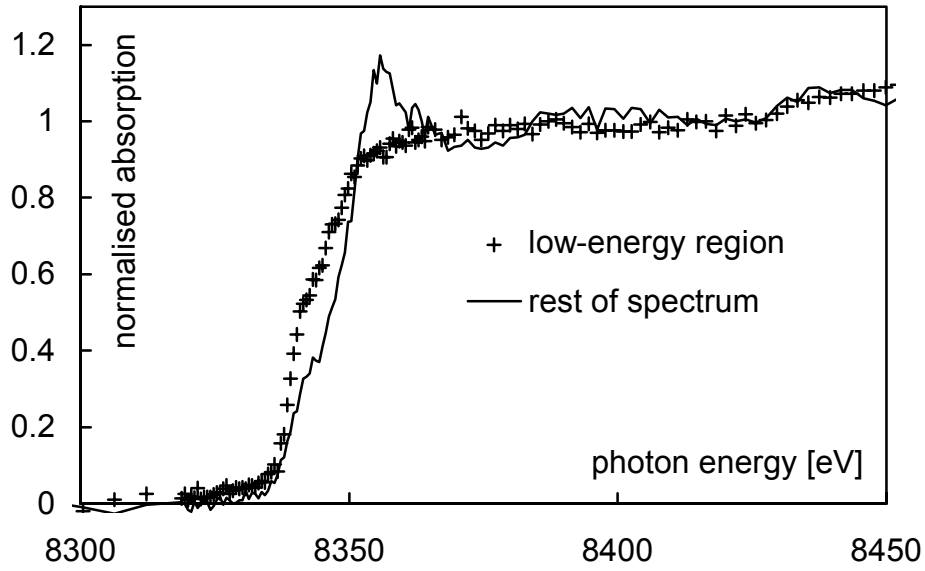

Figure 2.13. Pulse signal from low-energy region (E < 1000 eV, black crosses) compared to the information carried by the remaining pulse contributions. Note the much reduced, *quasi* non-existent fine-structure in the low-energy spectrum. See text for a possible explanation.

2.9. References

[1] R. Prins, D.C. Koningsberger, *Catalysis,* in: X-Ray Absorption. Principles, Applications, Techniques of EXAFS, SEXAFS and XANES (Chemical Analysis Vol.92), ed. by D.C. Koningsberger and R. Prins (John Wiley & Sons, New York/Chichester/Brisbane/Toronto/Singapore, 1988) 321.

[2] J. Evans, *EXAFS in the Study of Catalysts,* in: Catalysis Vol.8, (The Royal Society of Chemistry, Cambridge, 1989) 1.

[3] F.W.H. Kampers, T.M.J. Maas, J. van Grondelle, P. Brinkgreve, D.C. Koningsberger, Rev. Sci. Instrum. 60 (1989) 2635.

[4] A.J. Dent, G.N. Greaves, M.A. Roberts, G. Sankar, P.A. Wright, R.H. Jones, M. Sheehy, D. Madill, C.R.A. Catlow, J.M. Thomas, T. Rayment, , *Nucl. Instrum. Methods B* (1995) , in press

[5] G.P. Huffman, N. Shah, J. Zhao, F.E. Huggins, T.E. Hoost, S. Halvorsen, J. Goodwin, J. Catal. 151 (1995) 17.

[6] G.D. Moggridge, S.L.M. Schroeder, R.M. Lambert, T. Rayment, Nucl. Instrum. Methods B 97 (1995) 28.

[7] A. Caballero, A.R. González-Elipe, A. Fernández, J.M. Herrmann, H. Dexpert, F. Villain, J. Photochem. Photobiology A 78 (1994) 169.

[8] B.S. Clausen, L. Gråbæk, G. Steffensen, P.L. Hansen, H. Topsoe, Catal. Lett. 20 (1993) 23.

[9] S.M. Davis, G. Meitzner, D.A. Fischer, J.L. Gland, J. Catal. 142 (1993) 368.

[10] G. Sankar, P.A. Wright, S. Natarajan, J.M. Thomas, G.N. Greaves, A. Dent, B.R. Dobson, C.A. Ramsdale, R.H. Jones, J. Phys. Chem. 97 (1993) 9550.

[11] J.M. Thomas, G.N. Greaves, Catal. Lett. 20 (1993) 337.

[12] G. Sankar, S. Vasudevan, C.N.R. Rao, Chem. Phys. Lett. 620 (1986) 626.

[13] B.S. Clausen, H. Topsoe, Catalysis Today 9 (1991) 189.

[14] J.W. Couves, J.M. Thomas, D. Waller, R.H. Jones, A.J. Dent, G.E. Derbyshire, G.N. Greaves, Nature 354 (1991) 465.

[15] G.U. Kulkarni, G. Sankar, C.N.R. Rao, J. Catal. 131 (1991) 491.

[16] E.A. Shaw, T. Rayment, A.P. Walker, R.M. Lambert, T. Gauntlett, R.J. Oldman, A. Dent, Catalysis Today 9 (1991) 197.

[17] M. Kerkar, J. Robinson, A.J. Forty, Faraday Discuss. Chem. Soc. 89 (1990) 31.

[18] A.P. Walker, T. Rayment, R.M. Lambert, R.J. Oldman, J. Catal. 125 (1990) 67.

[19] T.L. Neils, J.M. Burlitch, J. Catal. 118 (1989) 79.

[20] S.M. Heald, *Design of an EXAFS Experiment,* in: X-Ray Absorption: Principles, Applications, Techniques of EXAFS, SEXAFS and XANES, ed. by D.C. Koningsberger and R. Prins (John Wiley & Sons, New York, Chichester, Brisbane, Toronto, Singapore, 1988) 87.

[21] G.E. Derbyshire, D. Bogg, A.J. Dent, R.C. Farrow, G.N. Greaves, W.I. Helsby, C. Morrell, C.A. Ramsdale, M.P. Wells, Rev. Sci. Instrum. 63 (1992) 790.

[22] A.J. Dent, M.P. Wells, R.C. Farrow, C.A. Ramsdale, G.E. Derbyshire, G.N. Greaves, J.W. Couves, J.M. Thomas, Rev. Sci. Instrum. 63 (1992) 903.

[23] M. Hagelstein, S. Cunis, R. Frahm, W. Niemann, P. Rabe, Physica B 158 (1989) 324.

[24] W. Niemann, B.S. Clausen, H. Topsoe, Ber. Bunsenges. Phys. Chem. 91 (1987) 1292.

[25] G. Sankar, C.N.R. Rao, T. Rayment, J. Mater. Chem. 1 (1991) 299.

[26] N.J. Shevchik, D.A. Fischer, Rev. Sci. Instrum. 50 (1979) 577.

[27] D.A. Fischer, G.G. Cohen, N.J. Shevchik, J. Phys. F 10 (1980) L139.

[28] G.G. Long, J. Kruger, D.R. Black, M. Kuryiama, J. Electroanal. Chem. 150 (1983) 603.

[29] G.G. Long, J. Kruger, D.R. Black, M. Kuryiama, J. Electrochem. Soc. 130 (1983) 240.

[30] T. Guo, M.L. denBoer, Phys. Rev. B 31 (1985) 6233.

[31] M.E. Kordesch, R.W. Hoffman, Phys. Rev. B 29 (1984) 491.

[32] G.G. Long, D.A. Fischer, J. Kruger, D.R. Black, D.K. Tanaka, G.A. Danko, Phys. Rev. B 39 (1989) 10651.

[33] Y.U. Idzerda, W.T. Elam, B.T. Jonker, G.A. Prinz, Phys. Rev. Lett. 62 (1989) 2480.

[34] D.T. Jiang, E.D. Crozier, Nucl. Instrum. Methods A 294 (1990) 666.

[35] T. Tyliszczak, A.P. Hitchcock, Physica B158 (1989) 335.

[36] G. Tourillon, E. Dartyge, A. Fontaine, M. Lemmonnier, F. Bartol, Phys. Letters A 121 (1987) 251.

[37] W.T. Elam, J.P. Kirkland, R.A. Neiser, P.D. Wolf, Phys. Rev. B 38 (1988) 26.

[38] K.I. Pandya, K. Yang, R.W. Hoffman, W.E. O'Grady, D.E. Sayers, J. Phys. (Paris) Colloque C8 (1986) 159.

[39] T. Girardeau, J. Mimault, M. Jaouen, P. Chartier, G. Tourillon, Phys. Rev. B 46 (1992) 7144.

[40] K.M. Kemner, Z. Wang, R.A. Mayanovic, B.A. Bunker, Nucl. Instrum. Methods B 71 (1992) 345.

[41] K.M. Kemner, A.J. Kropf, B.A. Bunker, Rev. Sci. Instrum. 65 (1994) 3667.

[42] I. Watanabe, H. Tanida, Anal. Sci. 11 (1995) 525.

[43] I. Watanabe, personal communication (1994)

[44] G.E. Derbyshire, A.J. Dent, B.R. Dobson, R.C. Farrow, A. Felton, G.N. Greaves, C. Morrell, M.P. Wells, Rev. Sci. Instrum. 63 (1992) 814.

[45] G.D. Moggridge, T. Rayment, R.M. Ormerod, M.A. Morris, R.M. Lambert, Nature 358 (1992) 658.

[46] S.L.M. Schroeder, G.D. Moggridge, R.M. Ormerod, T. Rayment, R.M. Lambert, Surf. Sci. Lett. 324 (1995) L371.

[47] W.P. Jesse, J. Sadaukis, Phys. Rev. 97 (1955) 1668.

[48] B. Sitar, G.I. Merson, V.A. Chechin, Y.A. Budagov, *Ionization Measurements in High Energy Physics (Springer Tracts in Modern Physics, Vol.124)* (Springer-Verlag, Berlin, Heidelberg, New York, etc. 1993).

[49] K. Kleinknecht, *Detectors for Particle Radiation* (Cambridge University Press, Cambridge, London, New York, 1986).

[50] A. Erbil, C.S. Cargill III, R. Frahm, R.F. Boehme, Phys. Rev. B 37 (1988) 2450.

[51] K.L. Bell, H.B. Gilbody, J.C. Hughes, A.E. Kingston, F.J. Smith, J. Phys. Chem. Ref. Data 12 (1983) 891.

[52] M.J. Berger, S.M. Seltzer, *NBS Internal Report 82-2550-A. Stopping Powers and Ranges of Electrons and Positrons (2nd Ed.)* (National Bureau of Standards, Washington, DC, 1983).

[53] M.J. Bedzyk, G. Materlik, Phys. Rev. B 32 (1985) 4228.

[54] M. Oversluizen, G.E. Derbyshire, C. Morrell, R. Farrow, B.R. Dobson, Rev. Sci. Instrum. 63 (1992) 924.

[55] R. Wilson, *Ionisation Counters,* in: Techniques of High Energy Physics, ed. by D.M. Ritson (Interscience Publishers, Inc. New York, 1961) 271.

[56] D.H. Wilkinson, *Ionization Chambers and Counters,* in: Cambridge Monographs in Physics, ed. by N. Feather and D. Shoenberg (Cambridge University Press, Cambridge, 1950)